

Mathematical Simulation of Transient Heat Transfer in a Two-Phase Closed Cylindrical Thermosiphon in Conditions of Convective Heat Exchange with an Environment

Dr. Abbas Alwi Sakhir Abed

Accepted 04 November 2013, Available online 01 December 2013, (Nov/Dec 2013 issue)

Abstract

Numerical simulation of mass transfer, momentum, and energy transport regimes in a two-phase closed cylindrical thermosiphon in conditions of convective heat exchange with an environment has been carried out. The mathematical model has been formulated in dimensionless variables such as stream function, vorticity, and temperature in cylindrical coordinates. Distributions of local thermo-hydrodynamic parameters reflecting influence of an environment have been obtained. Stages of energy transport from the evaporation zone to the condensation zone of the thermosiphon have been determined.

Keywords: Numerical simulation, Thermosiphon etc.

Introduction

Two-phase closed thermosiphon that basically is wickness gravitational heat pipe utilizes evaporation and condensation of working fluid within heat exchanger for transferring energy. Unlike usual heat pipe, which uses capillary force for returning fluid to evaporator, two-phase closed thermosiphon uses gravity to return condensate. It has simpler construction, less thermal resistance, higher efficiency and lower manufacturing cost. Due to these advantages two-phase closed thermosiphon is widely used in many fields, such as industrial heat recovery, cooling of electronic components and turbine blades, solar heating systems [1-3].

The most studies [4-8] are aimed to identify the characteristic properties of thermosiphons and to analyze their application. For example the research results of the influence of the working fluid filling ratio on the parameters of the stationary regimes during the heat transfer in two-phase closed thermosiphon based on the multivariate mathematical model are presented in [8]. Three variants of the interaction between the liquid film and the vapor channel are considered. Total intensity of the heat transfer in the fluid reservoir, caused by natural convection and bubble boiling is determined based on the combination of the effective (working) area and the heat transfer coefficients.

The new ratios of the effective area, based on the experimental results of the studies [4-7] have been proposed. The experimental studies of two different

geometric configurations of two-phase closed thermosiphon with nitrogen as the working fluid have shown fairly satisfactory correlation with the theoretical calculations. The main conclusion of this study is determining the diapason of variation of the filling ratio, where two-phase closed thermosiphon is able to be unsustainable and effectiveness. The influence of the heat input, the operating pressure and the geometrical configuration of thermosiphon in the diapason has been analyzed.

The experimental and numerical study [9] of various two-phase closed thermosiphons of small, medium and large scale has determined the real impact of the full drop of the system temperatures, the saturation temperature of the working fluid, the temperature and the speed of the coolant, the size of the condenser section, the volume of the fluid in the system of thermohydrodynamic structures, and the conditions for effective functioning of thermosiphons.

The investigation of the characteristics of the moderate regimes of two-phase closed thermosiphons based on the one-dimensional flow model using the correlation ratios determining the effects of the annular two-phase flow regime has been carried out in [10]. The heat transfer coefficient on the surface of the liquid film is determined in both laminar and turbulent approximations. The mathematical model includes differential laws of mass, momentum and energy conservation in the steam channel and in the liquid film. One of the major drawbacks of this model is lack of the influence of the environment as a result of neglecting

thermal conductivity of the walls, which can lead to different from the actual physical process results [11]. It should be noted that high intensity of the heat transfer mechanisms in presence of the phase change in thermosiphon leads to significant increase of the role of thermal conductivity in the hard surface even in the case of thin walls made from high conductive materials.

The mathematical modeling of the thermosiphon's transient modes on basis of the flat equations for laminar flow of compressible ideal gas is given in [12]. In the beginning, the presence of certain volume of liquid in the evaporator zone was neglected, which may significantly change the characteristics of the transient modes in thermosiphon. Instead, the critical volume of filling has been considered in the model which has been caused by the presence of sufficient amount of fluid wetting the walls of thermosiphon. It should be noted that the presence of critical mass supposes dependence of the working fluid from the heat power which is in some ways doesn't correlate with the working conditions of thermosiphons.

Statement

The boundary task of natural convection in the closed cylindrical region with the heat-conducting walls with defined thickness (figure 1) is considered in the presence of the local areas of evaporation and condensation which reflect the phase changing zones. In contrast to [13] this paper takes into account convective heat exchange with the environment on the boundary $z = L_z$, which reflects the real conditions of energy transfer from the lower to the upper layers of heat exchanger. Measurement of the convective heat transfer to the environment at the upper boundary of the solution area allows to evaluate efficiency and productivity of thermosiphon under the actual operating conditions.

During the mathematical simulation it is assumed that the external surface of the vertical walls are adiabatic, and at the lower boundary $z = 0$ the constant temperature is maintained [13]. The considered geometry of the task and the boundary conditions allow to eliminate the influence of the azimuth coordinate and to analyze the process of mass, momentum and energy transfer in the axisymmetric statement. During the calculation experiments it has been suggested that the thermal properties of the wall's material, steam and liquid do not depend on the temperature, and the flow regime is laminar. Steam has been considered as viscous, heat conducting, Newtonian fluid satisfying the Boussinesq approximation. To investigate the hydrodynamic conditions in the liquid film, the analytical approach has been used which is described in [14].

The mathematical model was formulated using the following assumptions:

- the convective heat transfer with the environment on the external borders of the vertical walls is considered

negligibly small compared with intense longitudinal thermal conductivity;

- the flows in the steam channel and in the liquid film are considered in laminar approaching;

- it is suggested that steam is saturated and is able to be considered as ideal gas due to its very low pressure.

Taking into account the defined assumptions, the main transport equations of mass, momentum and energy in the dimensionless variables "electricity function - vorticity - temperature" in cylindrical coordinates in the "steam channel - liquid film" system will take the form [13]:

$$\frac{\partial \Omega_1}{\partial \tau} = \frac{\partial(U_1 \Omega_1)}{\partial R} + \frac{\partial(V_1 \Omega_1)}{\partial Z} = \sqrt{\frac{Pr_1}{Ra_1}} \left(\nabla^2 \Omega - \frac{\Omega_1}{R^2} \right) + \frac{\partial \theta_1}{\partial R} \tag{1}$$

$$\nabla^2 \Psi_1 - \frac{2}{R} \frac{\partial \Psi_1}{\partial R} = -R \Omega_1 \tag{2}$$

$$\frac{\partial \theta_1}{\partial \tau} + \frac{\partial(U_1 \theta_1)}{\partial R} + \frac{\partial(V_1 \theta_1)}{\partial Z} = \frac{1}{\sqrt{Ra_1 Pr_1}} \nabla^2 \theta_1 - \frac{U_1 \theta_1}{R} \tag{3}$$

$$V_2 = L_z^2 \frac{\rho g_z - \varphi}{4 \mu_2} R^2 + C_1 \ln R + C_2 \tag{4}$$

$$\Psi_2 = \int_{r_1/z_2}^{(r_1+r_2)/z_2} V_2 dR \tag{5}$$

$$\frac{\partial \theta_2}{\partial \tau} = \frac{1}{\sqrt{Ra_2 Pr_2}} \nabla^2 \theta_2 \tag{6}$$

The heat-transfer equation in the thermosiphon's walls:

$$\frac{\partial \theta_3}{\partial F_0} = \nabla^2 \theta_3 \tag{7}$$

where

$$Ra_1 = g_z \beta \Delta T z_2^3 / \nu a_1, \quad Ra_2 = g_z \beta \Delta T z_2^3 / \nu a_2 -$$

The Rayleigh numbers in the steam channel and in the liquid film; ν – coefficient of kinematic viscosity; a – temperature conductivity coefficient;

$Pr_1 = \nu_1 / a_1, Pr_2 = \nu_2 / a_2$ – the Prandtl numbers of steam

and liquid; $\nabla^2 = \frac{1}{R} \frac{\partial}{\partial R} \left(R \frac{\partial}{\partial R} \right) + \frac{\partial^2}{\partial Z^2}$ – the immense

Laplacian operator; $F_0 = \frac{a_3 t_0}{z_2^2}$ – the Fourier number; φ – barometric gradient. Constants C_1 and C_2 are defined from the boundary conditions.

The Nusselt number reflecting intensity of the heat transfer on the phase boundary steam – solid wall $Z = z_1/z_2$ is defined from the equation:

$$Nu = \int_0^{r_1/z_2} \frac{\partial \theta}{\partial z} dR \tag{8}$$

The immense boundary conditions for the equations 1–7 are defined in the form of:

$$R = 0, \quad 0 \leq Z \leq L_z/z_2, \quad \frac{\partial \theta}{\partial R} = 0, \quad \Psi = 0 \tag{9}$$

$$R = \frac{L_r}{z_2}, \quad 0 \leq Z \leq L_z/z_2, \quad \frac{\partial \theta}{\partial R} = 0 \tag{10}$$

$$R = \frac{r_1}{z_2}, \quad \frac{z_1}{z_2} \leq Z \leq \frac{z_1 + z_2}{z_2}, \quad \frac{\partial \theta_1}{\partial R} = \lambda_{2,1} \frac{\partial \theta_2}{\partial R},$$

$$\theta_1 = \theta_2, \quad \left. \frac{\partial \psi}{\partial R} \right|_1 = \left. \frac{\partial \psi}{\partial R} \right|_2, \quad \Omega_1 = \mu_{2,1} \Omega_2 \quad (11)$$

$$R = \frac{r_1 + r_2}{z_2}, \quad \frac{z_1}{z_2} \leq Z \leq \frac{z_1 + z_2}{z_2}, \quad \frac{\partial \theta_2}{\partial R} = \lambda_{3,2} \frac{\partial \theta_3}{\partial R},$$

$$\theta_2 = \theta_3, \quad \left. \frac{\partial \psi}{\partial R} \right| = \psi = 0 \quad (12)$$

$$Z = 0, \quad 0 \leq R \leq L_r/z_2, \quad \theta = \theta_h \quad (13)$$

$$Z = \frac{L_z}{z_2}, \quad 0 \leq R \leq L_r/z_2, \quad \frac{\partial \theta}{\partial Z} = Bi(\theta_e - \theta) \quad (14)$$

$$Z = \frac{z_1}{z_2}, \quad 0 \leq R \leq r_1/z_2,$$

$$\frac{\partial \theta_3}{\partial R} = \lambda_{1,3} \frac{\partial \theta_1}{\partial R} + Q_{ev} w_{ev}, \quad \theta_3 = \theta_1 \quad (15)$$

$$Z = \frac{z_1 + z_2}{z_2}, \quad 0 \leq R \leq r_1/z_2,$$

$$\frac{\partial \theta_1}{\partial R} = \lambda_{3,1} \frac{\partial \theta_3}{\partial R} - Q_{con} w_{con}, \quad \theta_1 = \theta_3 \quad (16)$$

where $\lambda_{2,1} = \lambda_2/\lambda_1$ – relative thermal coefficient of conductivity; $\mu_{2,1} = \mu_2/\mu_1$ – relative dynamic viscosity coefficient; Q_{ev} , Q_{con} and w_{ev} , w_{con} – dimensionless heats and speed of evaporation and condensation; $Bi = \alpha L_z/\lambda_3$ – the Biot number.

The formulated boundary task with the appropriate initial and boundary conditions has been solved by the finite difference method [13 - 17].

The developed method has been tested on the model problem. The flat laminar convective flow of the viscous heat-conducting fluid [18] in the closed cylindrical cavity has been considered. On the vertical walls and on the upper horizontal wall the constant heat flow has been maintained. The lower horizontal wall is adiabatic.

The following figures show the comparison of the streamlines and the temperature fields at the different values of Rayleigh number with the numerical results [18].

The results presented on figures 2 - 4 clearly show that the established mathematical model and the used numerical algorithm of solutions lead to fairly appropriate correlation with the results of the other authors.

Analysis of the taken results

The numerical simulations have been performed for a cylindrical thermosiphon with steel walls and water as working fluid. The following geometrical characteristics of the thermosiphon have been selected: height - 100 mm, radius - 25 mm, wall thickness - 2 mm.

Figures 5 – 8 show the characteristic current lines, the fields of velocity and temperature at the various Rayleigh numbers. The increase of Ra leads to the intensification of convective the heat transfer in the steam channel. The growth of the evaporable liquid is happen upon the condition that the velocity of fluid in the liquid film is constant. It should be noted that in the condensation zone the flow is separated - some steam condenses and makes a flow in the liquid film; the rest of the steam reflects forming of the circulation area in the steam zone. At $Ra = 10^3$ (figure 5), the main mechanism of energy transfer is thermal conductivity, so low speed of circulation is observed. The time of the heat transfer from the evaporation zone to the condensation zone is large enough that incommensurate with the actual conditions of thermosiphons.

The increase of the thermal lift tenfold (figure 6) leads to the formation of the recirculation zone in the lower part of the exchanger. The last statement reflects the formation of the dead flow heat area which prevents intensive transportation of energy to the upper layers of the thermosiphon. Further increase of the Rayleigh number (figures 7, 8) appears in the displacement of the vortex in vertical direction to the condensation zone, which may also lead to reduced efficiency of the analyzed object.

Figure 9 shows the temperature profiles in the cross section $R = 0$ for the different values of the Rayleigh number. The increase of the temperature drop in the steam channel leads to the increase of the temperature on the cylinder axis. The most significant changes are observed at $10^4 < Ra < 10^5$, due to both the formation of the thermal plume and the stability in the recirculation zone in the steam channel (figure 7).

Figure 10 shows the dependence of the average Nusselt number from the Rayleigh number on the boundary $Z = z_1/z_2$. The low-intensity modes of energy transfer at $Ra < 5 \cdot 10^4$ should be noted, reflecting the dominance of the conductive the heat transfer mechanisms. Further increasing of the temperature lift leads to the significant increase of the Nusselt number Nu.

Figure 10,b shows the unsteadiness of the analyzed process. The change of the average Nusselt number with time is most significant at the initial stage $0 < \tau \leq 5$. At $\tau > 5$ the thermally stabilized regime is achieved.

The vertical velocity profiles at the different cross-sections are shown in figure 11. The distributions on figure 11 confirm once again the formation of the low-intensity convective flow at $Ra = 10^4$. With distance from the evaporation boundary the increase of the steam flow velocity is observed, that characterizes the presence of the downstream temperature pressure.

The increase of the Rayleigh number (figure 11,b) leads to the significant increase of the steam flow rate in the center of the channel, and also appears with the increase of the size of the area with the downward steam

flows close to the liquid film. The last statement characterizes the intensification of the heat transfer in the analyzed heat exchanger.

The comparison of the taken distributions of the isotherms and the streamlines with the case of the constant temperature maintained on the boundary $Z = L_z/2$ [13] reflects the significant influence of the type of boundary conditions at the initial step. Over time the differences become negligible, due to the influence of the thermosiphon's envelope as well as the achievement of the steady-state energy transfer mode. Figure 12 shows the comparison of the temperature profiles in the typical cross-sections of the thermosiphon. Using the boundary conditions determining the actual mechanisms of heat exchange with the environment appears in the temperature decrease due to the low thermal resistance of the protection solid walls.

Conclusions

The multivariate numerical analysis of the unsteady modes of the conjugate heat-gravitational convection in the cylindrical thermosiphon with convective heat exchange with the environment has been carried out. The distributions of the streamlines, the velocity and temperature fields are calculated which characterize the features of the analyzed flow and the heat transfer modes at $Ra = 10^3-10^6$, $Pr = 0,7$, $0 \leq \tau \leq 100$. The features of the formation of thermo-hydrodynamic regimes during the alteration of the temperature lift in the analyzed object have been established. It has been shown that for $0 < \tau \leq 5$ the significant changes in the average Nusselt number on the evaporation surface have been arranged. The significant differences in the local distribution of the streamlines and isotherms with the case of the constant temperature on the outer surface have been found out.

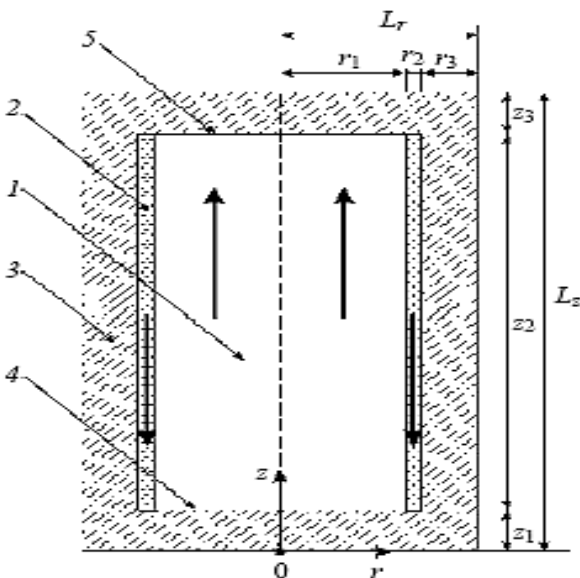


FIG. 1. Search space: 1 – steam; 2 – liquid film; 3 – metal carcass; 4 – evaporation surface; 5 – condensation surface.

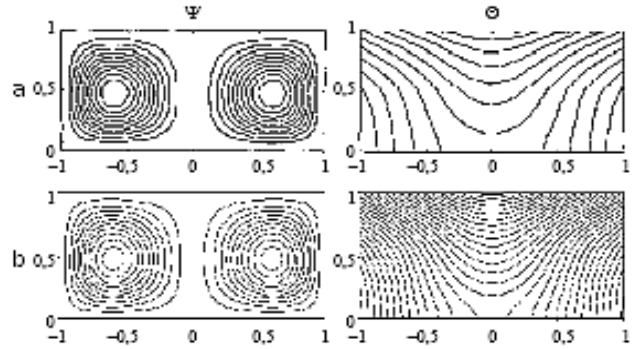


FIG. 2. Streamlines Ψ and temperature fields Θ at $Pr = 0,7$, $Ra = 10^3$: the results [18] – a, the taken results – b.

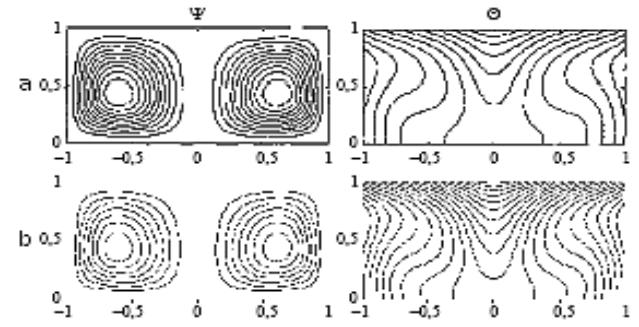


FIG. 3. Streamlines Ψ and temperature fields Θ at $Pr = 0,7$, $Ra = 10^4$: the results [18] – a, the taken results – b.

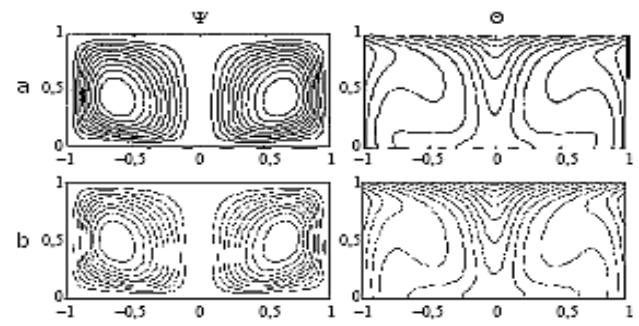


FIG. 4. Streamlines Ψ and temperature fields Θ at $Pr = 0,7$, $Ra = 10^5$: the results [18] – a, the taken results – b.

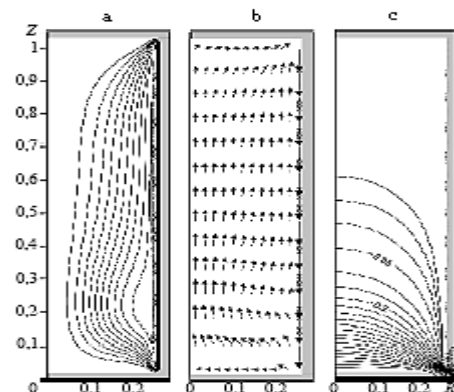


FIG. 5. Streamlines (a), velocity (b) and temperature (c) fields at $Ra = 10^3$.

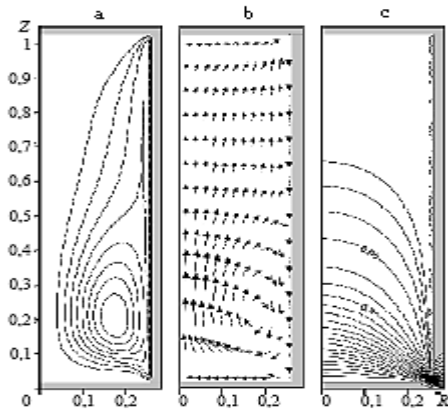


FIG. 6. Streamlines (a), velocity (b) and temperature (c) fields at $Ra = 10^4$.

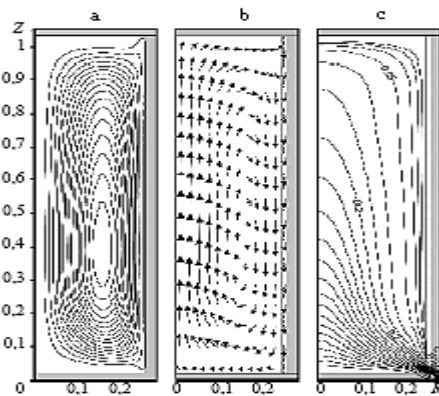


Fig 7. Streamlines (a), velocity (b) and temperature (c) fields at $Ra = 10^5$.

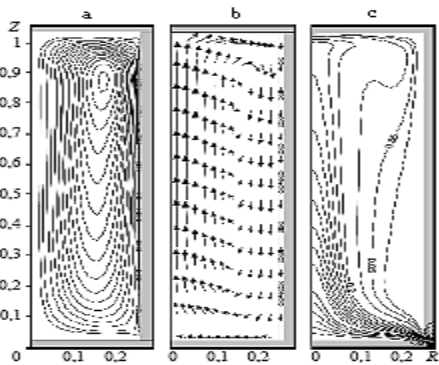


FIG. 8. Streamlines (a), velocity (b) and temperature (c) fields at $Ra = 10^6$.

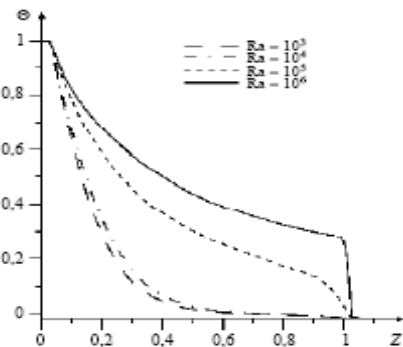


FIG. 9. Temperature profiles in section $R = 0$.

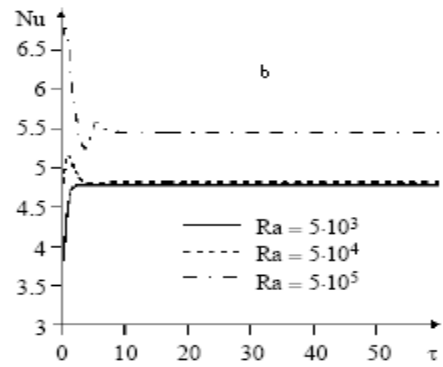
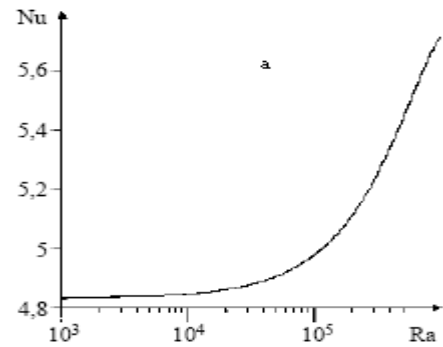


FIG. 10. Dependence of the average Nusselt number from the Rayleigh number (a) and from nondimensional time (b).

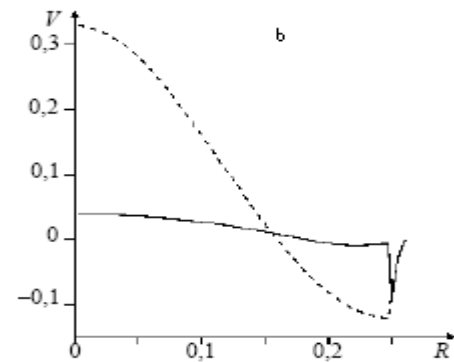
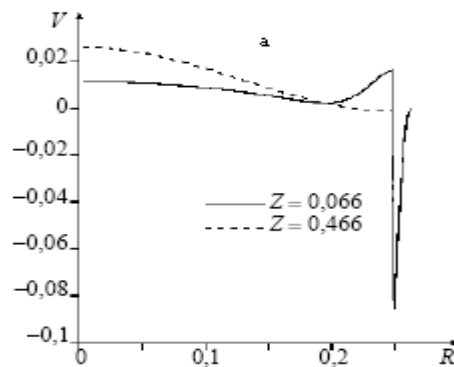


FIG. 11. The profile of the vertical velocity component in the different cross-sections $Z = const$ at $Ra = 10^4$ (a) and at $Ra = 10^5$ (b)

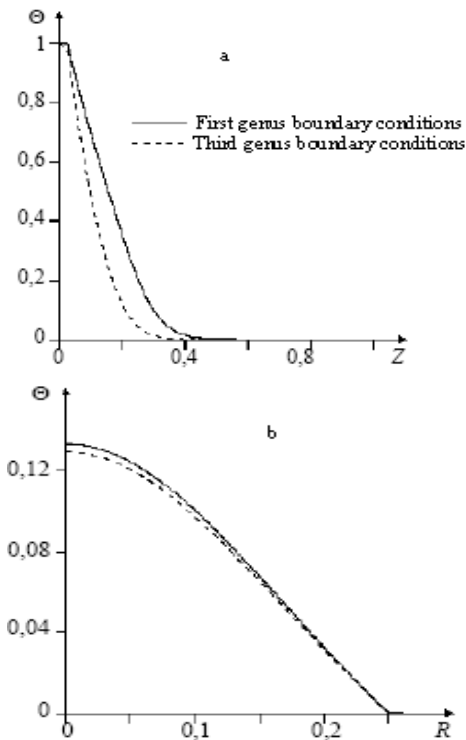


FIG. 12. Temperature profiles at $Ra = 10^5$ in the cross-section $R = 0$ at $\tau = 2$ (a) ; $Z = 0,9$ at $\tau = 60$ (b)

References

- [1]. Esen M., Esen H. Experimental investigation of a two-phase closed thermosiphon solar water heater // *Solar Energy*. 2005. V. 79. P. 459–468.
- [2]. Desrayaud G., Fichera A., Marcoux M. Numerical investigation of natural circulation in a 2D-annular closed-loop thermosiphon // *Int. J. Heat Fluid Flow*. 2006. V. 27. P. 154–166.
- [3]. Bakiev T.A., Usupov S.T. Prospects of thermosiphons' usage in the gas industry // *Materials of the scientific-technical conference*. M.:OOO «IRC Gazprom», 2005. P. 16–22.
- [4]. Imura H., Ssasaguchi K., Kozai H. Critical heat flux in a closed two phase thermosiphon // *Int. J. Heat Mass Transfer*. 1983. V. 26. P. 1181–1188.
- [5]. Shiraishi M., Kikuchi K., Yamarcishi T. Investigation of heat transfer characteristics of a two phase closed thermosiphon // *Proc. Fourth Intern. Heat Pipe Conf.* 1981. P. 95–104.
- [6]. Ueda T., Miyashita T., Chu P.H. Heat transport characteristics of a closed two-phasethermosiphon // *Trans. JSME*. 1988. Part B 54. V. 506. P. 2848–28
- [7]. El-Genk M.S., Saber H.H. Heat transfer correlations for small, uniformly heated liquid pools // *Intern. J. Heat Mass Transfer*. 1998. V. 41. P. 261–274.
- [8]. Jiao B., Qiu L.M., Zhang X.B., Zhang Y. Investigation on the effect of filling ratio on the steady-state heat transfer performance of a vertical two-phase closed thermosiphon // *Appl. Therm. Eng.* 2008. V. 28. P. 1417–1426.
- [9]. Seok-Ho Rhi. An Experimental and Analytical Study on Two-Phase Loop Thermosyphons. Very Small to Very Large Systems // *The Ottawa-Carleton Institute for Mechanical and Aeronautical Engineering*. D.S.Thesis. Canada, 2000.
- [10]. Reed J.G., Tien C.L. Modeling of the Two-Phase Closed Thermosiphon // *ASME. J. Heat Transfer*. 1987. V. 109. P. 722–730.
- [11]. Sheremet M.A. The influence of cross effects on the characteristics of heat and mass transfer in the conditions of conjugate natural convection // *J. Engineering Thermophysics*. 2010. V. 19, № 3. P. 119–127.
- [12]. Harley C., Faghri A. A complete transient two-dimensional analysis of two-phase closed thermosyphons including the falling condensate film // *ASME. J. Heat Transfer*. 1994. V. 116. P. 418–426.
- [13]. Kuznetsov G.V., Al-Ani M.A., Sheremet M.A. Numerical analysis of the effect of the temperature drop on the modes of energy transport in a closed cylindrical two-phase thermosiphon // *Proceedings of the Tomsk polytechnic university*. 2010. V. 317. № 4. P. 13–19.
- [14]. Semenov P. Flows in thick layers // *GTF*. 1944. V. 14. № 7–8. P. 427–437.
- [15]. Rouch P. *Calculative hydrodynamics*. M.: Mir, 1980. 616 p.
- [16]. Samarskiy A.A. *Theory of difference schemes*. M.: Nauka, 1977. 656 p.
- [17]. Paskonov V.M., Polegaev V.I., Chidov L.A. *Numerical simulation of heat and mass transfer*. M.: Nauka, 1984. 288 p.
- [18]. Lembre A., Petit J.P. Laminar natural convection in a laterally heated and upper cooled vertical cylindrical enclosure // *Int. J. Heat Mass Transfer*. 1998. V. 41. P. 2437–2454.